AGU PUBLICATIONS

Radio Science

RESEARCH ARTICLE
10.1002/2014RS005422

Special Section:
Beacon Satellite Symposium 2013

Occurrence of equatorial spread *F* during intense geomagnetic storms

S. Ray[1], B. Roy[2], and A. Das[2]

[1]Institute of Radio Physics and Electronics, University of Calcutta, Kolkata, India, [2]S. K. Mitra Center for Research in Space Environment, University of Calcutta, Kolkata, India

Key Points:
- Geomagnetic storms during 1996–2005 are ordered in terms of Dst and IMF B_z
- Effects of PPE during intense storms are studied from global ion density plots
- Longitudes of occurrence of ESF in response to PPE are predicted from IMF B_z

Correspondence to:
S. Ray,
sarbanir@yahoo.com

Citation:
Ray, S., B. Roy, and A. Das (2015), Occurrence of equatorial spread *F* during intense geomagnetic storms, *Radio Sci.*, *50*, 563–573, doi:10.1002/2014RS005422.

Received 7 MAR 2014
Accepted 19 MAY 2015
Accepted article online 21 MAY 2015
Published online 2 JUL 2015

Abstract Equatorial spread *F* (ESF) has been observed in response to the prompt penetration of magnetospheric electric field to equatorial latitudes during intense (minimum $Dst \leq -100$ nT; $B_z \leq -10$ nT for at least 3 h) magnetic storms using global ion density plots of Defense Meteorological Satellite Program (DMSP) over nearly one solar cycle (1996–2005). Geostationary amplitude scintillation observations from Calcutta at VHF and L band for 1996–2005 and GPS amplitude scintillation measurements during 2004–2005 from the Indian Satellite Based Augmentation System Geostationary and GPS Navigation Outlay (GPS Aided GEO Augmented Navigation) network of stations all over India have been used to corroborate the DMSP observations. Subsequent to the time of southward interplanetary magnetic field B_z crossing −10 nT for an intense storm, it has been observed that within 4 h, ESF is generated at a longitude where the local time is dusk.

1. Introduction

The cause of geomagnetic storms are strong dawn-to-dusk electric fields generated due to the passage of southward directed interplanetary magnetic field (IMF) B_z, past the Earth for sufficiently long intervals of time [*Gonzalez et al.*, 1994]. The southward IMF B_z causes a change in the field-aligned region 1 current which in turn causes the dawn-to-dusk polar cap potential to increase suddenly. The region 2 current which is related to an inner magnetospheric electric field directed from dusk to dawn and shields the middle- and low-latitude ionosphere from high-latitude electric fields cannot change as fast as the region 1 current. This causes an "undershielding" condition when the high-latitude electric field penetrates into the low latitudes, a phenomenon popularly known as prompt penetration of high-latitude electric field (PPE) [*Wolf et al.*, 2007; *Basu et al.*, 2010]. The phenomenon of PPE had frequently been observed in the 1970s and1980s [*Fejer*, 1986], but these fields were difficult to distinguish from the disturbance dynamo electric fields which were of longer time scale. *Fejer and Scherliess* [1995] statistically combined Jicamarca data to quantitatively define the average response to a step function increase in polar cap potential, and the results were compared with Rice Convection Model (RCM) results. The expected duration of PPE has been investigated by several workers. *Jaggi and Wolf* [1973] reported from simulations that the nightside electric field decreased in 10 min but complete shielding occurred in ~2 h. Comparing with Jicamarca data [*Spiro et al.*, 1988; *Fejer et al.*, 1990], the RCM penetration electric fields did not last as long as the observed fields. Later, it has been established from RCM simulations that there can be considerable penetration throughout the main phase of a major magnetic storm [*Garner et al.*, 2004].

The *F* region plasma irregularities with scale sizes ranging from meters to hundreds of kilometers in the equatorial ionosphere are commonly known as equatorial spread *F* [*Li et al.*, 2012]. At equatorial latitudes, the geomagnetic field **B** is almost parallel to the Earth's surface, and during the day, the *E* region dynamo electric field **E** is eastward. This gives rise to the resultant vertical $\mathbf{E} \times \mathbf{B}$ drift which lifts the *F* region plasma upward at the magnetic equator. The uplifted plasma then moves along the magnetic field lines in response to gravity and pressure-gradient forces to off-equatorial locations. As a result, the equatorial anomaly is formed with a trough in ionization density at the magnetic equator and two crests around 15°–20° north and south magnetic latitudes. Although near sunset, plasma densities and dynamo electric fields in the *E* region decrease, and the anomaly begins to weaken; however, at this local time, a dynamo develops in the *F* region. Polarization charges within the conductivity gradients at the terminator enhance the electric field after sunset. The postsunset electric field moves the ionospheric plasma upward, thus intensifying the anomaly crests. During these hours, a rapid uplifting of the *F* region and the steepening of the bottomside gradient give rise to the Rayleigh-Taylor instability which allows irregularities to form. The

Table 1. Intense Geomagnetic Storms During 1996–2005

Storm	Peak *Dst* Value	Time (UT)	Date	Time of IMF B_z Crossing −10 nT (UT)	Date
06–07 Aug 1998	−138	11:00	06 Aug 1998	06:74	6 Aug 1998
13–15 Jan 1999	−112	23:00	13 Jan 1999	15:00	13 Jan 1999
06–08 Apr 2000	−288	00:00	07 Apr 2000	16:07	6 Apr 2000
11–13 Aug 2000	−235	09:00	12 Aug 2000	01:52	12 Aug 2000
28–30 Oct 2000	−127	03:00	29 Oct 2000	20:24	28 Oct 2000
19–21 Mar 2001	−149	13:00	20 Mar 2001	11:93	19 Mar 2001
31 Mar to 02 Apr 2001	−387	08:00	31 Mar 2001	03:77	31 Mar 2001
31 Oct to 02 Nov 2001	−106	10:00	01 Nov 2001	20:37	31 Oct 2001
17–18 Apr 2002	−127	07:00	18 Apr 2002	09:48	17 Apr 2002
18–19 Jun 2003	−141	09:00	18 Jun 2003	04:50	18 Jun 2003
17–19 Aug 2003	−148	15:00	18 Aug 2003	03:84	18 Aug 2003
29–31 Oct 2003	−383	22:00	30 Oct 2003	17:94	29 Oct 2003
11–15 Feb 2004	−109	17:00	11 Feb 2004	10:59	11 Feb 2004
22–23 Jul 2004	−101	02:00	23 Jul 2004	19:85	22 Jul 2004
07–12 Nov 2004	−373	06:00	08 Nov 2004	22:33	7 Nov 2004
29–31 May 2005	−138	13:00	30 May 2005	05:69	30 May 2005
12–13 Jun 2005	−106	00:00	13 Jun 2005	16:01	12 Jun 2005

irregularities can grow to become large structures of plasma depletions often called equatorial plasma bubbles [*Kelley et al*., 1976; *McClure et al*., 1977; *Alfonsi et al*., 2013]. A satellite signal passing through a plasma bubble experiences fluctuations of amplitude and phase popularly known as scintillations.

The PPE is eastward during the daytime to the dusk sector and westward in the midnight to the dawn sector [*Basu et al*., 2001a]. It is known that the eastward prompt penetration electric field becomes enhanced near sunset due to the day-to-night conductivity gradient. The enhanced eastward electric fields near dusk generate the Rayleigh-Taylor plasma instability at equatorial *F* region heights and favor the formation of

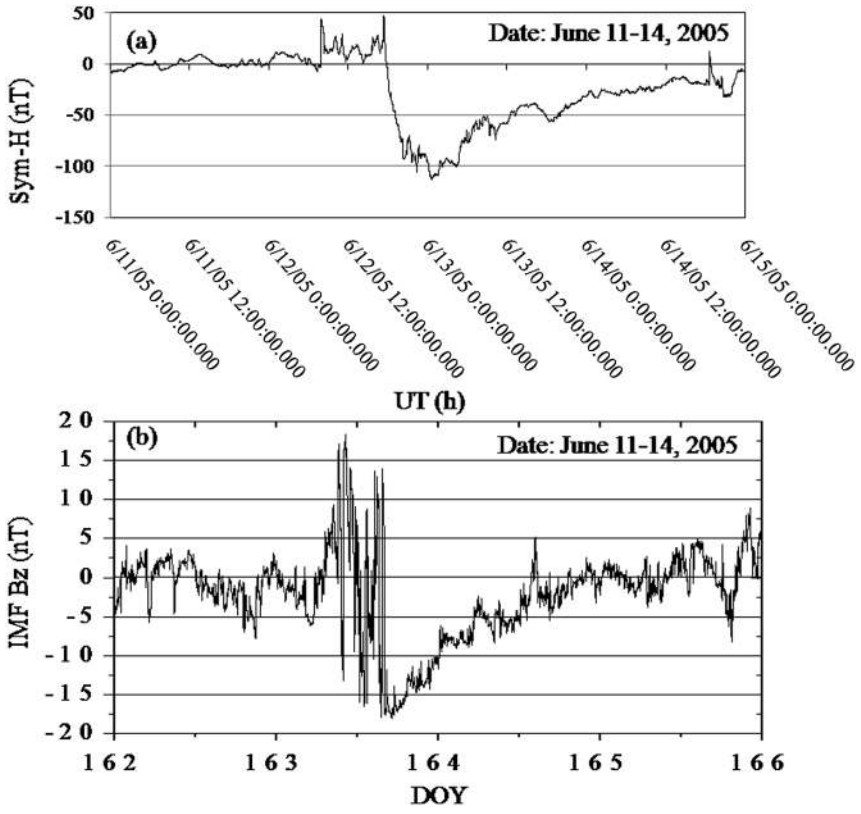

Figure 1. (a) Variation of *SYM-H* (nT) observed during 11–14 June 2005. (b) Variation of IMF B_z (nT) observed during 11–14 June 2005.

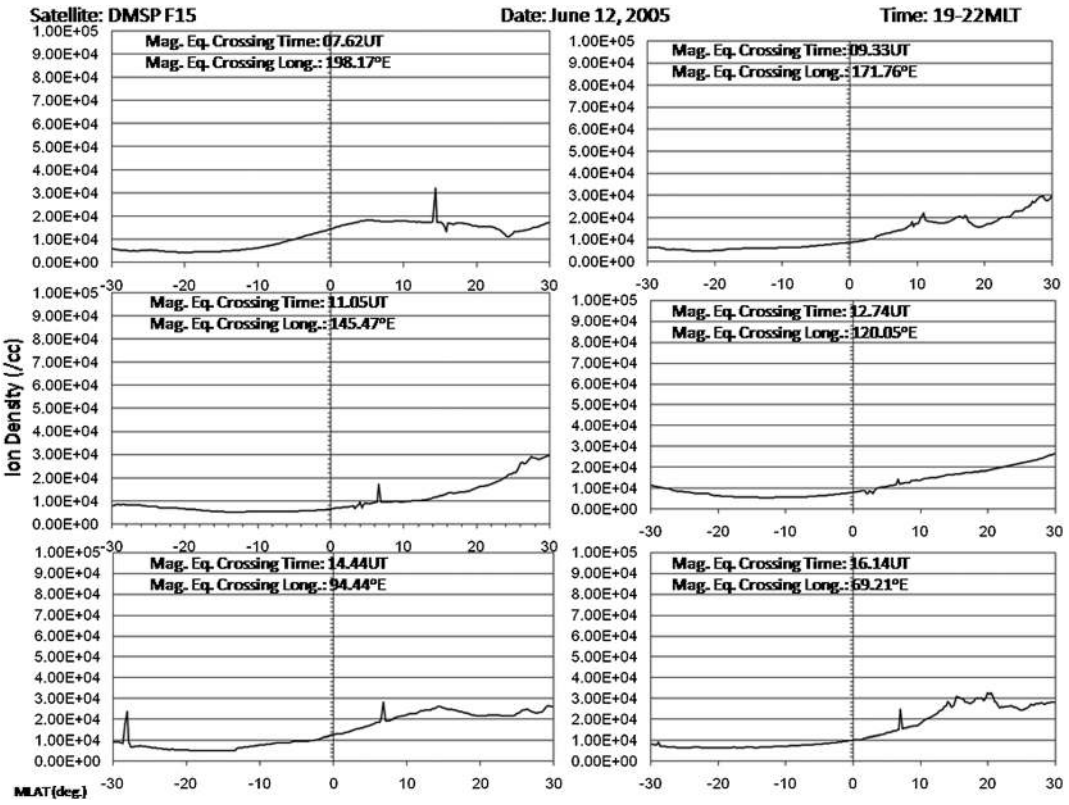

Figure 2. Plots of total ion density (/cc) observed by DMSP F15 during 12 June 2005.

plasma bubbles and irregularities of electron density that result in scintillations of satellite signals. Since the phenomenon of scintillations has detrimental effects on satellite-based communication and navigation systems, penetration electric fields have become a major space weather issue. *Greenspan et al*. [1991] and *Basu et al*. [2001b] have shown that the enhanced eastward electric field during the main phase of major magnetic storms can almost eliminate the equatorial *F* layer by lifting it so high that the plasma diffuses down along the magnetic field lines into the midlatitudes.

Basu et al. [2010] studied the longitudinal confinement of VHF scintillations and plasma bubbles in the equatorial ionosphere, using Scintillation Network Decision Aid network and Defense Meteorological Satellite Program (DMSP) satellite in situ measurements during the main phase of 30 large (rate of change of $Dst \leq -50$ nT/h and minimum $Dst \leq -100$ nT) magnetic storms in solar cycle 23. They also showed that from the knowledge of UT interval of the main phase of a storm, it is possible to determine the dusk sector corresponding to the storm main phase and thereby specify the longitude interval over which bubbles and scintillations should be detected.

This paper presents a study of the response of equatorial ionosphere to the prompt penetration of magnetospheric electric field to equatorial latitudes during intense (minimum $Dst \leq -100$ nT; $B_z \leq -10$ nT for at least 3 h) magnetic storms using global ion density plots of Defense Meteorological Satellite Program (DMSP) over nearly one solar cycle (1996–2005). Geostationary amplitude scintillation observations from Calcutta at VHF and L band for 1996–2005 and GPS amplitude scintillation measurements during 2004–2005 from the GPS Aided GEO Augmented Navigation (GAGAN) network of stations all over India have been used to corroborate the DMSP observations. Using the time of southward IMF B_z crossing -10 nT for a storm, the longitude of equatorial spread *F* (ESF) occurrence resulting from prompt penetration of electric field have been predicted.

2. Data

The storms under study have been ordered both with respect to *Dst* and B_z. The *Dst* indices have been obtained from the World Data Center for Geomagnetism, Kyoto (url address: http://swdcwww.kugi.kyoto-u.ac.jp/). *SYM-H*

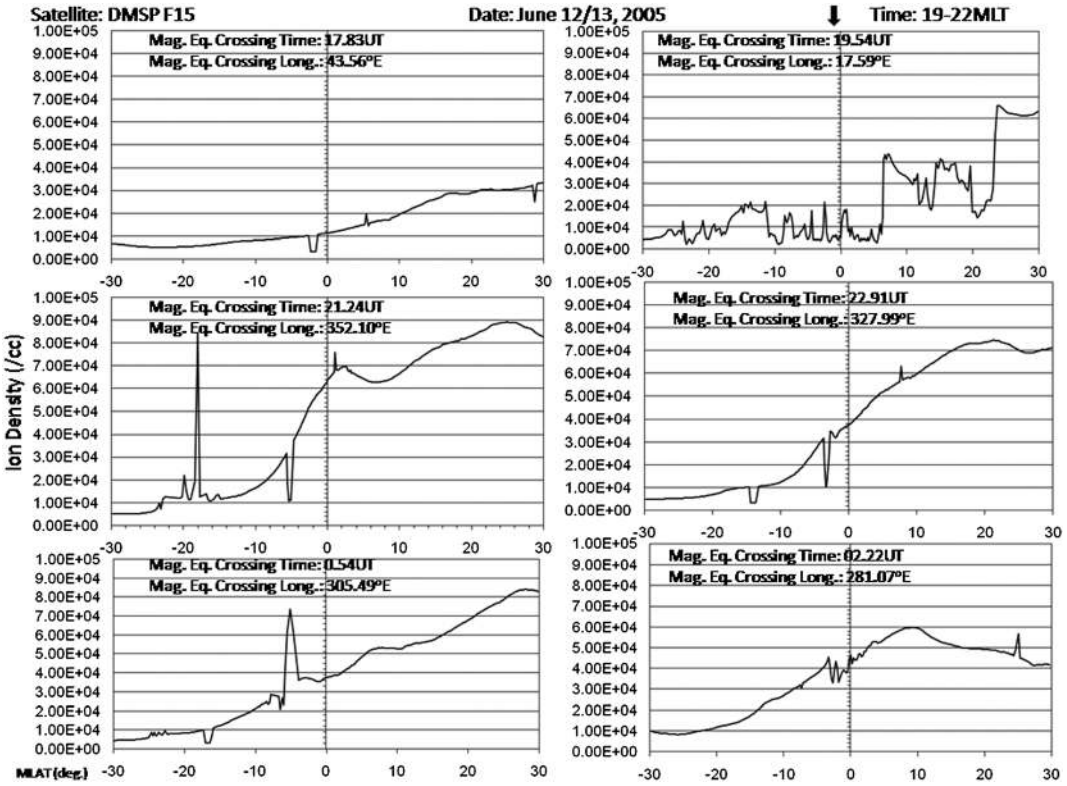

Figure 3. Plots of total ion density (/cc) observed by DMSP F15 during 12–13 June 2005. The black arrow indicates the frame showing the presence of irregularities.

index, the 1 min values of *Dst*, have been considered for individual storms. IMF B_z data at 64 s sampling interval have been obtained from the Advanced Composition Explorer (ACE) satellite (url address: http://www.srl.caltech.edu/ACE/). ACE orbits the L1 libration point which is a point of Earth-Sun gravitational equilibrium about 1.5×10^6 km from the Earth. The IMF measurements have been time shifted to the nose of the bow shock to obtain a better representation of the solar wind-magnetospheric interaction. In situ total ion density measurements at 4 s sampling interval by Sun-synchronous DMSP F12, F14, and F15 satellites at altitude 840 km, period of 96 min, which cross the magnetic equator during 19:00–22:00 magnetic local time (MLT), are available from the website (url address: http://cindispace.utdallas.edu/DMSP). Amplitude of the L band carrier signal (1537.528 MHz) from INMARSAT (350 km subionospheric point 21.08° N, 86.59°E geographic; 28.74° magnetic dip angle) and VHF carrier signal (244.156 MHz) from FLEETSATCOM (350 km subionospheric point: 21.10°N, 87.25°E geographic; 28.65° magnetic dip angle) have regularly been recorded at Calcutta (22.58°N, 88.38°E geographic; 32° magnetic dip angle) since 1990 and 1981, respectively. In situ ion density data from DMSP satellites and ground-based geostationary scintillation measurements at VHF and L band from Calcutta have been analyzed for all storms under study. Data from 18 GAGAN reference stations located all over the Indian subcontinent ranging from 08.47°N–31.09°N latitude, 72.18°E–92.72°E longitude, and magnetic dip angle 0.91°–47.43° sampled at 1 Hz were available for the period of 2004–2005 in a processed form. The S_4 indices corresponding to patches of amplitude scintillations observed on GPS links from different GAGAN stations during the storms of 2004–2005 were scaled at 1 min intervals.

3. Results and Discussions

During the period of 1996–2005, 17 storms could be identified which satisfied the criteria of intense storms (minimum $Dst \leq -100$ nT; $B_z \leq -10$ nT for at least 3 h). The storm particulars are shown in Table 1. One such storm occurred during 12–13 June 2005 when the commencement took place at 07:75 UT on 12 June and

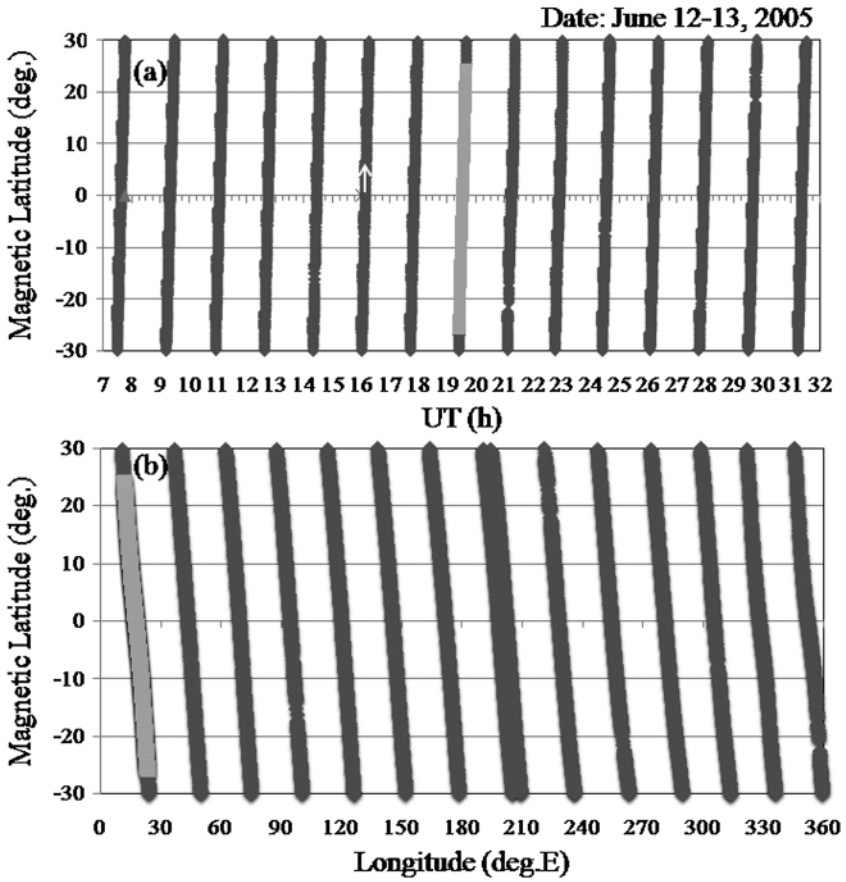

Figure 4. Presence of irregularities (indicated by the light grey portion) in DMSP tracks represented in (a) time and (b) longitude during the intense magnetic storm of 12–13 June 2005. The white arrow in Figure 4a indicates the time of southward IMF B_z crossing −10 nT. ESF generation is at 19:54 UT, 3.53 h after the time of IMF B_z crossing −10 nT at 16:01 UT, at a longitude 17.64° whose local time is 20:72.

ended at 21:00 UT on 13 June. Figure 1a shows the variation of *SYM-H* during 11–14 June 2005. The peak *SYM-H* of magnitude −138 nT was observed at 00:63 UT on 13 June. Figure 1b shows the variation of IMF B_z during the storm. IMF B_z turned southward in excess of 10 nT at 16:01 UT on 12 June, reached a minimum of −18.06 nT at 17:13 UT, and remained southward with values less than 10 nT for 08.15 h until 00:16 UT on 13 June which occurred during the main phase of the storm.

In order to observe the effect of the enhanced PPE at dusk on the equatorial ionosphere globally, in situ ion density from successive DMSP transits crossing the equator between 19:00 and 22:00 MLT throughout each storm have been plotted for magnetic latitudes −30° to 30°. Figures 2 and 3 show the plots of total ion density for orbits of DMSP F15 with equator crossing times ranging from 07:62 UT on 12 June to 02:22 UT on 13 June. The usual absence of ESF during the low sunspot number years of 2005 (monthly smoothed sunspot number for June 2005: 28.8) is observed, except for a sudden outburst of irregularities about the magnetic equator around 17.59°E (shown with an arrow in Figure 3), at 19:54 UT corresponding to a local time of 20:71. Figure 4 shows the tracks with respect to time (Figure 4a) and longitude (Figure 4b), respectively, of the passes for which the ion density have been plotted in Figures 2 and 3. The light grey portions of the tracks indicate the occurrence of equatorial irregularities. It is observed that the irregularities are confined to a narrow longitude zone at 17.59°. Comparing the time of occurrence of irregularities during this particular storm with the time of southward IMF B_z crossing −10 nT, it is found that the irregularities occur with a delay of 3.53 h after southward B_z exceeded −10 nT during the storm main phase. The geostationary links at VHF and L band received from Calcutta did not record any scintillation activity during this storm.

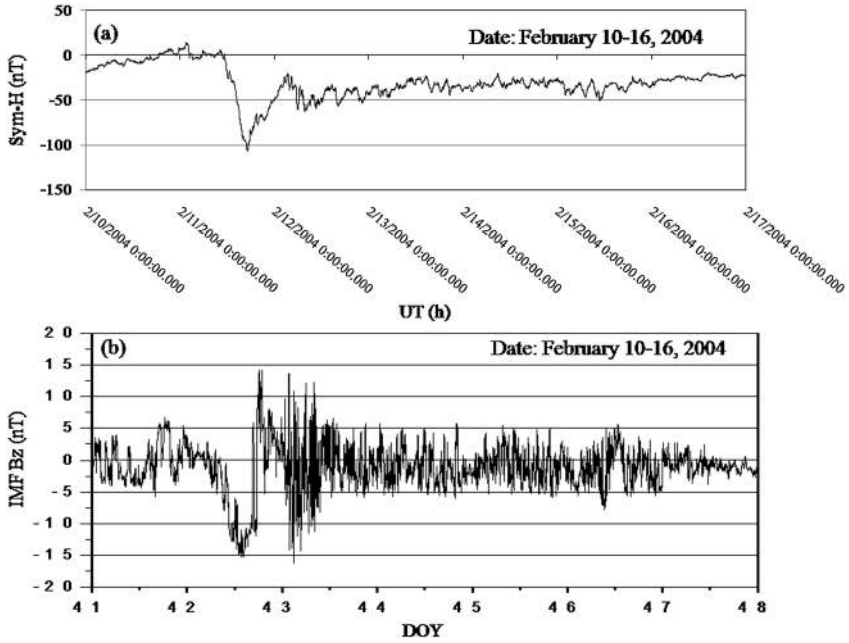

Figure 5. (a) Variation of *SYM-H* (nT) observed during 10–16 February 2004. (b) Variation of IMF B_z (nT) observed during 10–16 February 2004.

Another storm, during which geostationary scintillations were recorded at Calcutta, started at 11:00 UT on 11 February 2004 and ended at 00:00 UT on 15 February 2004. The storm attained a peak *SYM-H* of −100 nT at 16:95 UT on 11 February (Figure 5). The IMF B_z dipped below −10 nT at 10:59 UT and remained below −10 nT until 11:45 UT reaching a maximum of −12.87 nT at 11:29 UT. There was again a second maximum of −15.33 nT at 14:31 UT when the IMF B_z remained below −10 nT from 12:71 UT to 16:19 UT. The total ion density for the DMSP F15 satellite transiting during 11–15 February is plotted in the same way as described above. Figures 6 and 7 show ion density plots for passes with equator crossing time from 10:96 UT to 22:83 UT on 11 February. It is observed that patches of irregularities (shown with arrows in Figures 6 and 7) occurred when the satellite crossed the equator at 12:66 UT and continued until 17:74 UT, coinciding with the main phase of the storm and around the time of maximum ring current intensification. During this time interval, the satellite encompassed longitudes from 128.21°E to 51.88°E, covering the

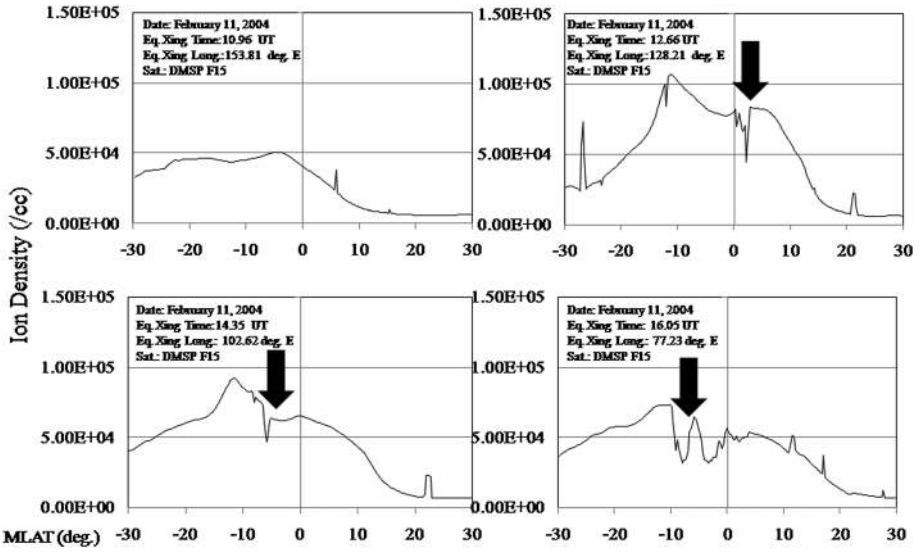

Figure 6. Plots of total ion density (/cc) observed by DMSP F15 during 11 February 2004. The black arrow indicates frames showing presence of irregularities.

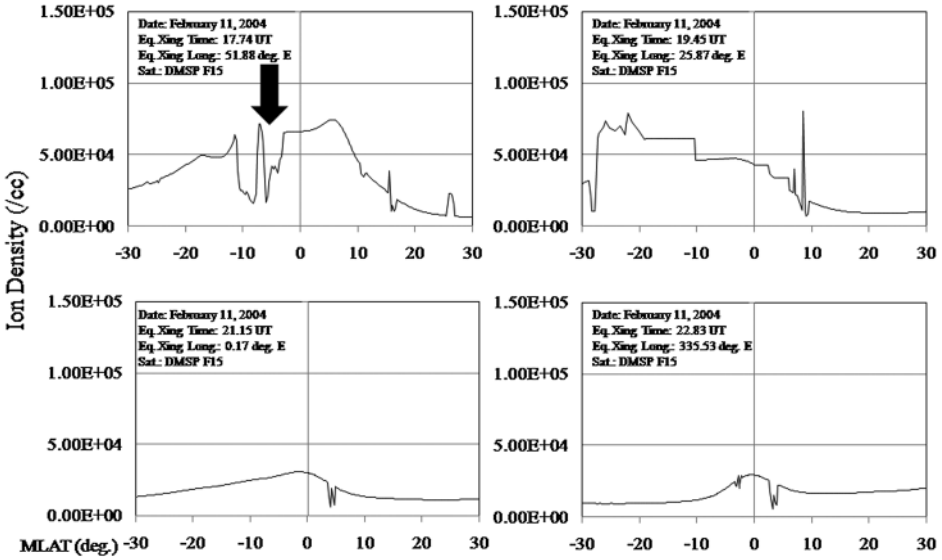

Figure 7. Same as Figure 6.

Indian subcontinent completely and prompting comparison with scintillation measurements from Indian stations. Figure 8 shows the location of these stations.

Patches of intense scintillations were observed at Calcutta on the VHF link from 16:25 UT to 19:75 UT with a maximum S_4~1.07. Simultaneously, moderate scintillations were observed on the L band link between 16:00 UT and 16:75 UT with a peak in S_4~0.30. Figure 9a shows the variation of S_4 during the storm. To observe scintillations at Calcutta which is located near the crest of the equatorial anomaly, the plasma bubbles have to rise at least to a height of 750 km at the magnetic equator to map down along the field lines to a mean ionospheric height of 350 km at the location of Calcutta.

Out of the 18 GAGAN reference stations recording GPS amplitude scintillations, data were available for only six stations, namely, Aizwal (23.83°N, 92.62°E geographic; 34.87° magnetic dip angle), Guwahati (26.12°N,

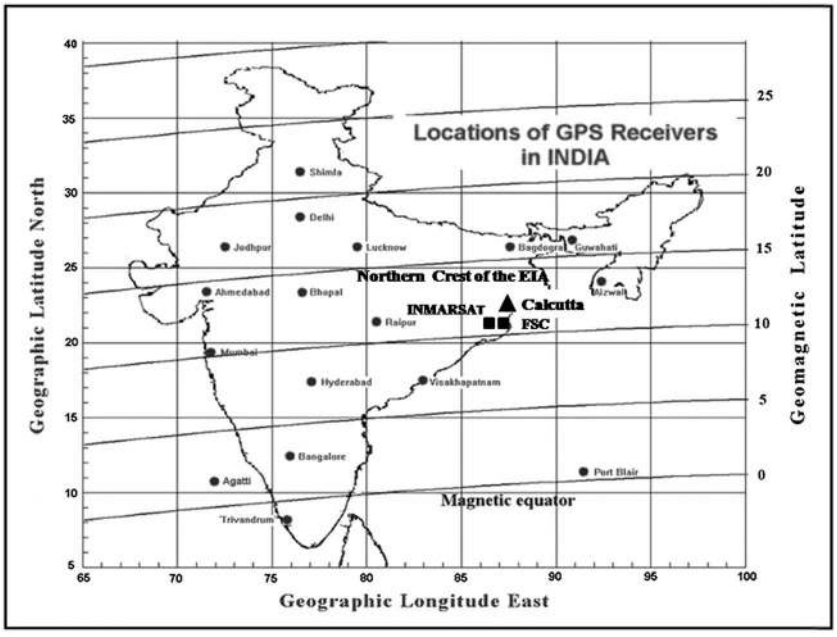

Figure 8. Map of India showing the location of GAGAN reference stations, subionospheric points of Inmarsat, and FSC. The magnetic equator and the northern crest of the equatorial anomaly are also indicated.

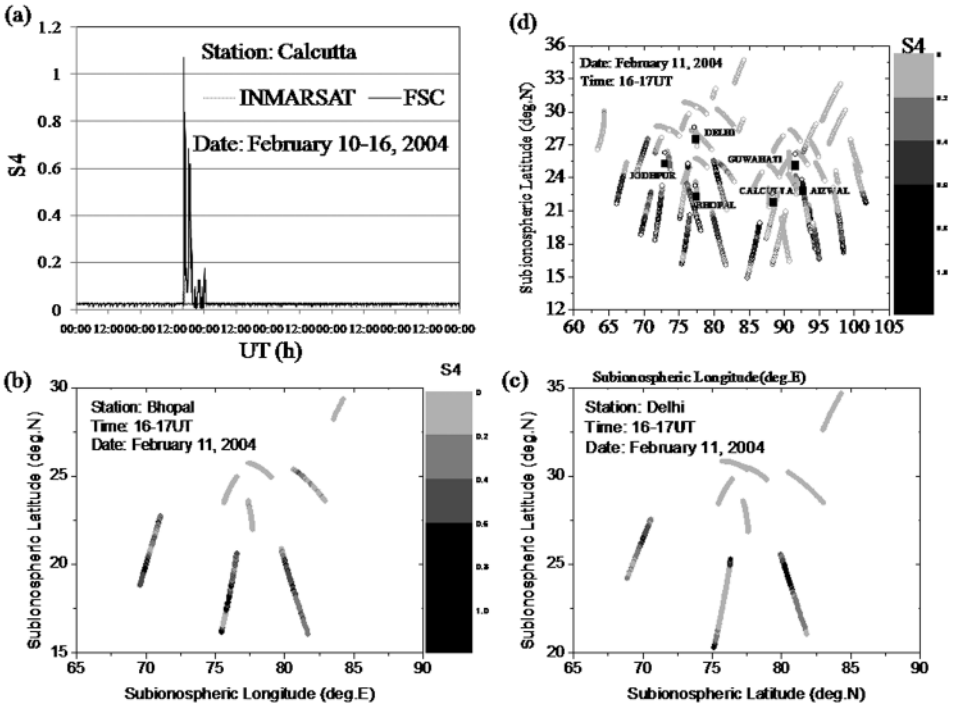

Figure 9. (a) Variation of S_4 index observed on Inmarsat and FSC links during 10–16 February 2004. (b) GPS satellite tracks at 350 km observed from Bhopal during 16:00–17:00 UT on 11 February 2004. (c) GPS satellite tracks at 350 km observed from Delhi during 16:00–17:00 UT on 11 February 2004. (d) GPS satellite tracks at 350 km observed from Jodhpur, Delhi, Bhopal, Calcutta, Guwahati, and Aizwal during 16:00–17:00 UT on 11 February 2004. The bold portions in Figures 9b–9d indicate regions of scintillation with $S_4 > 0.6$.

91.59°E geographic; 39.08° magnetic dip angle), Calcutta (22.58°N, 88.38°E geographic; 32° magnetic dip angle), Bhopal (23.28°N, 77.34°E geographic; 33.95° magnetic dip angle), Delhi (28.58°N, 77.21°E geographic; 43.5° magnetic dip angle), and Jodhpur (26.26°N, 73.05°E geographic; 39.79° magnetic dip angle) during the storm of 11–15 February. Intense scintillations with S_4 in excess of 0.6 were observed in all the six stations on 11 February. All the other nights during the storm, namely, 12–14 February, did not show any scintillation activity in any of the stations. The local times of Aizwal and Guwahati are UT + 06.13 h, that of Calcutta: UT + 05.87 h, Bhopal and Delhi: UT + 05.13 h, and Jodhpur: UT + 04.87 h. Aizwal, situated near the anomaly crest, recorded intense scintillations in three GPS satellite links located between 94°E–104°E and 16°N–21°N 350 km subionospheric during 16:00–17:00 UT. In the next hour 17:00–18:00 UT, nearing midnight, when the irregularities responsible for L band scintillations have started decaying, only one satellite located at 92°E between 21°N and 22°N observed scintillations with intensity $S_4 > 0.6$. From Guwahati, situated poleward of the anomaly crest, scintillations of similar intensity were recorded by one satellite link around 23°N to 24°N and 93°E to 94°E. GPS measurements from Calcutta, situated near the crest of the equatorial anomaly, showed that intense scintillations were observed in one GPS satellite link sampling the ionosphere between 16°N–20°N and 85°E–86°E during 16:00–17:00 UT. Bhopal, also situated near the anomaly crest, recorded scintillations with S_4 in excess of 0.6 during 15:00–16:00 UT and 16:00–17:00 UT. In the first hour, intense scintillations were observed in links between 15°N–24°N latitude and 70°E–80°E longitude. In the next hour, patches of intense scintillations were observed in locations between 15°N–21°N latitude and 70°E–82°E longitude. Delhi, located poleward of the anomaly crest location, observed intense scintillations during 16:00–17:00 UT in 20°N to 26°N latitudes and between 70°E and 82°E longitudes. The 350 km subionospheric tracks of GPS satellites observed during 16:00–17:00 UT are shown for Bhopal and Delhi in Figures 9b and 9c, respectively. The black portions of the tracks indicate regions of intense scintillations ($S_4 > 0.6$). Basically, Bhopal and Delhi are situated along the same longitude (77°E), the former near the anomaly crest and the latter poleward. The plasma bubble that has been observed by both these stations has also been observed by the DMSP F15 transit crossing the equator at 16:05 UT at 77.23°E longitude (fourth frame of Figure 6). Jodhpur, located just poleward of the

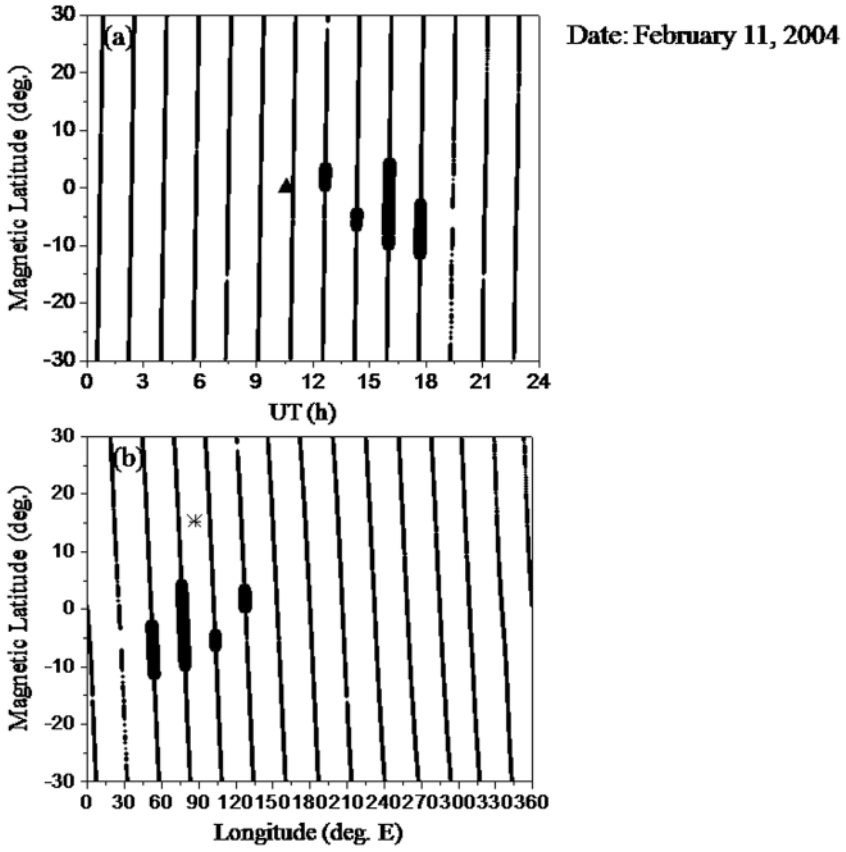

Figure 10. Presence of irregularities (indicated by the bold portion) in DMSP F15 tracks represented in (a) time and (b) longitude during 11 February 2004. The triangle in Figure 10a indicates the time of southward IMF B_z crossing −10 nT. ESF generation is at 12:66 UT and continued until 17:74 UT, the onset being 2.07 h after the time of IMF B_z crossing −10 nT at 10:59 UT, at a longitude 128.21° whose local time is 21:21. ESF was observed in successive passes continuing until 51.88°E longitude. The cross and plus symbols in Figure 10b indicate, respectively, the subionospheric points of Inmarsat and FSC.

anomaly crest at a more western longitude, recorded intense scintillations, in a short patch at 24°N, 76°E during 15:00–16:00 UT and more extensively in a region covering 66°E to 78°E longitude and 18°N to 24°N latitude during 16:00–17:00 UT. So, in summary, the ESF that has been observed about the magnetic equator at longitudes 128.21°E through 51.88°E from in situ ion density measurements by DMSP F15, subsequent to the southward turning of the IMF B_z during the storm of 11 February, has been simultaneously observed by the GAGAN stations near the crest of the anomaly and poleward from GPS amplitude scintillation measurements covering a longitude zone of 104°E to 70°E (Figure 9d). Figure 10 summarizes the observations of the storm of 11–15 February 2004.

The index S_4 is the ratio of the root-mean-square deviation of the signal power and the average power [*Briggs and Parkin*, 1963], while the scintillation index (SI) (dB) [*Whitney et al*., 1969] has been defined as the decibel excursions between the third peak up from the minimum and third peak down from the maximum signal levels. The level of scintillation intensity ($S_4 > 0.6$) observed on 11 February corresponds to SI greater than 15 dB. For communication engineers, an SI > 15 dB implies a fade depth of 12 dB or more. So if a receiver has a fade margin of less than 12 dB, fades greater than 12 dB will not be accommodated by the receiver and thus result in loss of link in a situation of intense scintillation activity described above.

During the present study with 17 intense storms, of which two have been illustrated above, it has been observed from DMSP data that during all the storms, irregularities occur during the main phase with a time difference from the time of southward IMF B_z crossing −10 nT in a longitude zone where the local time is dusk (19:00–22:00 MLT).

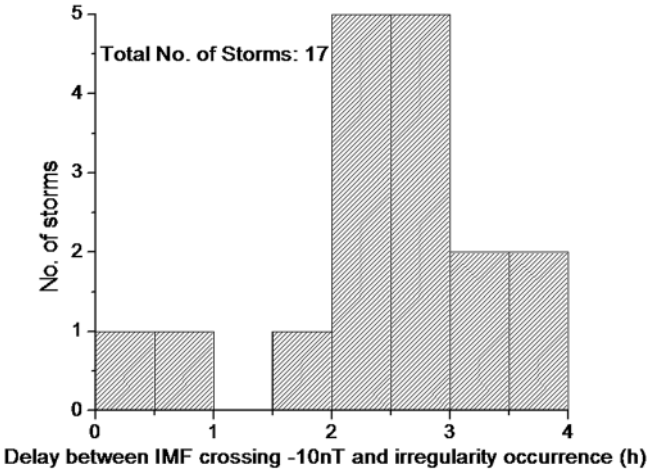

Figure 11. Distribution of delay between the time of southward IMF B_z crossing −10 nT and the time of ESF occurrence. The total number of intense storms is 17.

From the occurrence of ESF for 17 intense storms, a distribution of this delay (Figure 11) has been obtained. It is observed from Figure 11 that 11.77% of storms have delay within 1 h, 17.65% have delay within 2 h, and 76.47% of the storms have delay less than 3 h. The time delay between the southward IMF B_z crossing −10 nT and onset of ESF occurrence gives a measure of the time scale of undershielding. One limitation of this analysis is that the DMSP transits have an orbital period of 96 min. So if the onset of ESF is in between two successive transits, the lead time for prediction is decreased by a maximum of 96 min. This will affect only 11.77% of the storms which have delay less than 96 min.

Figure 12 shows the world map for the occurrence of ESF for 17 intense geomagnetic storms during 1996–2005. Each colored bar plotted at the magnetic equator indicates the longitude of onset of ESF during an intense geomagnetic storm. The colors of the bars have been indexed according to the time interval in UT when the IMF B_z crossed −10 nT. From Figure 12, it is evident that for an intense storm with the time of southward IMF B_z crossing −10 nT between 18:00 and 24:00 UT (shown with different shades of blue), ESF occurs around 300°–0° longitude. Similarly, for storms with time of southward IMF B_z crossing −10 nT in other UT sectors, the longitudes of ESF occurrence are illustrated.

Geostationary scintillation measurements from Calcutta during the 17 storms under study reveal that there were only two storms, namely, that of 19–21 March 2001 and 11–15 February 2004, for which scintillations were observed in the dusk sector in the main phase subsequent to southward turning of IMF B_z. For the other storms, the time period of undershielding did not correspond to the dusk sector for Calcutta.

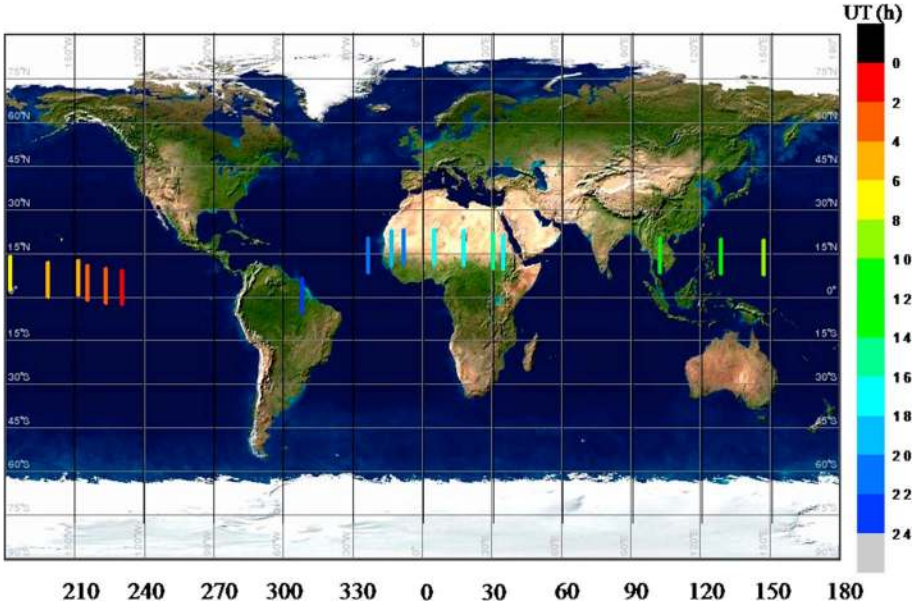

Figure 12. World map showing the occurrence of ESF for 17 intense storms. The positions of the color bars indicate the longitude at which ESF occurred for the first time, and the colors of the bars indicate the UT interval during which the southward IMF B_z crossed −10 nT.

4. Conclusions

Based on analysis of 17 intense geomagnetic storms, it has been established that during intense geomagnetic storms, ESF will be generated within 4 h of southward IMF B_z crossing −10 nT when undershielding condition prevails in that longitude sector for which the local time is dusk. Knowing the time of southward IMF B_z crossing −10 nT real time from the ACE satellite, for any geomagnetic storm, it will be possible to predict the longitude sector likely to be affected by ESF occurrence during that storm. Earlier studies [*Martinis et al*., 2005; *Abdu et al*., 2009; *Rastogi et al*., 2012] have shown that during the IMF B_z southward period, undershielding electric field promptly penetrate to equatorial latitudes with eastward polarity in the sunset sector causing large vertical drift at the time of prereversal enhancement, thereby leading to enhanced instability growth and ESF generation. When the IMF B_z turns northward, large overshielding westward electric field leads to total suppression of prereversal enhancement and ESF. But forecasting the time of ESF generation and the affected longitude sector from the time of southward turning of IMF B_z has not been reported earlier.

The global distribution of longitudes affected by ESF generated due to penetration electric field (Figure 12) is skewed. It would be interesting to investigate why the time of southward turning of IMF B_z and consequently the time period of undershielding has a preferred UT sector.

Acknowledgments

The authors thankfully acknowledge the Center for Space Physics at the University of Texas at Dallas and the U.S. Air Force for providing the DMSP thermal plasma data, the ACE MAG Instrument Team for the IMF B_z data, and the World Data Center at Kyoto University for *Dst* and *SYM-H* data. This work has been sponsored by Indian Space Research Organization, Department of Space, Government of India through projects. The authors are grateful to Ashish Dasgupta for the useful discussions.

References

Abdu, M. A., E. A. Kherani, I. S. Batista, and J. H. A. Sobral (2009), Equatorial evening prereversal vertical drift and spread *F* suppression by disturbance penetration electric fields, *Geophys. Res. Lett.*, *36*, L19103, doi:10.1029/2009GL039919.

Alfonsi, L., L. Spogli, M. Pezzopane, V. Romano, E. Zuccheretti, G. De Franceschi, M. A. Cabrera, and R. G. Ezquer (2013), Comparative analysis of spread-*F* signature and GPS scintillation occurrences at Tucuman, Argentina, *J. Geophys. Res. Space Physics*, *118*, 4483–4502, doi:10.1002/jgra.50378.

Basu, S., S. Basu, K. M. Groves, H. -C. Yeh, S.-Y. Su, F. J. Rich, P. J. Sultan, and M. J. Keskinen (2001a), Response of the equatorial ionosphere in the South Atlantic region to the great magnetic storm of July 15, 2000, *Geophys. Res. Lett.*, *28*(18), 3577–3580, doi:10.1029/2001GL013259.

Basu, S., et al. (2001b), Ionospheric effects of major magnetic storms during the International Space Weather Period of September and October 1999: GPS observations, VHF/UHF scintillations, and in situ density structures at middle and equatorial latitudes, *J. Geophys. Res.*, *106*(A12), 30,389–30,413, doi:10.1029/2001JA001116.

Basu, S., S. Basu, E. MacKenzie, C. Bridgwood, C. E. Valladares, K. M. Groves, and C. Carrano (2010), Specification of the occurrence of equatorial ionospheric scintillations during the main phase of large magnetic storms within solar cycle 23, *Radio Sci.*, *45*, RS5009, doi:10.1029/2009RS004343.

Briggs, B. H., and I. A. Parkin (1963), On the variation of radio star and satellite scintillations with zenith angle, *J. Atmos. Terr. Phys.*, *25*(6), 339–366.

Fejer, B. G. (1986), Equatorial ionospheric electric fields associated with magnetospheric disturbances, in *Solar Wind-Magnetosphere Coupling*, edited by Y. Kamide and J. A. Slavin, pp. 519–545, Terra Science Publ. Co., Tokyo.

Fejer, B. G., and L. Scherliess (1995), Time-dependent response of equatorial ionospheric electric fields to magnetospheric disturbances, *Geophys. Res. Lett.*, *22*(7), 851–854, doi:10.1029/95GL00390.

Fejer, B. G., R. W. Spiro, R. A. Wolf, and J. C. Foster (1990), Latitudinal variation of perturbation electric fields during magnetically disturbed periods: 1986 SUNDIAL observations and model results, *Ann. Geophys.*, *8*, 441–454.

Garner, T. W., R. A. Wolf, R. W. Spiro, W. J. Burke, B. G. Fejer, S. Sazykin, J. L. Roeder, and M. R. Hairston (2004), Magnetospheric electric fields and plasma sheet injection to low L-shells during the 4–5 June 1991 magnetic storm: Comparison between the Rice Convection Model and observations, *J. Geophys. Res.*, *109*, A02214, doi:10.1029/2003JA010208.

Gonzalez, W. D., J. A. Joselyn, Y. Kamide, H. W. Kroehl, G. Rosoker, B. T. Tsuruani, and V. M. Vasyliunas (1994), What is a geomagnetic storm?, *J. Geophys. Res.*, *99*(A4), 5771–5792, doi:10.1029/93JA02867.

Greenspan, M. E., C. E. Rasmussen, W. J. Burke, and M. A. Abdu (1991), Equatorial density depletions observed at 840 km during the great magnetic storm of March 1989, *J. Geophys. Res.*, *96*(A8), 13,931–13,942, doi:10.1029/91JA01264.

Jaggi, R. K., and R. A. Wolf (1973), Self-consistent calculation of the motion of a sheet of ions in the magnetosphere, *J. Geophys. Res.*, *78*(16), 2852–2866, doi:10.1029/JA078i016p02852.

Kelley, M. C., G. Haerendel, H. Kappler, A. Valenzuela, B. B. Balsley, D. A. Carter, W. L. Ecklund, C. W. Carlson, B. Hausler, and R. Torbett (1976), Evidence for a Rayleigh-Taylor type instability and upwelling of depleted density regions during equatorial spread *F*, *Geophys. Res. Lett.*, *3*(8), 448–451, doi:10.1029/GL003i008p00448.

Li, G., B. Ning, M. A. Abdu, W. Wan, and L. Hu (2012), Precursor signatures and evolution of post-sunset equatorial spread-*F* observed over Sanya, *J. Geophys. Res.*, *117*, A08321, doi:10.1029/2012JA017820.

Martinis, C. R., M. J. Mendillo, and J. A. Aarons (2005), Toward a synthesis of equatorial spread *F* onset and suppression during geomagnetic storms, *J. Geophys. Res.*, *110*, A07306, doi:10.1029/2003JA010362.

McClure, J. P., W. B. Hanson, and J. H. Hoffman (1977), Plasma bubbles and irregularities in the equatorial ionosphere, *J. Geophys. Res.*, *82*(A7), 2650–2656, doi:10.1029/JA082i019p02650.

Rastogi, R. G., H. Chandra, A. C. Das, R. Sridharan, B. W. Reinisch, and K. Ahmed (2012), Effects of a magnetic cloud simultaneously observed on the equatorial ionosphere in midday and midnight sectors, *Earth Planets Space*, *64*(4), 353–360.

Spiro, R. W., R. A. Wolf, and B. G. Fejer (1988), Penetration of high-latitude-electric-field effects to low latitudes during SUNDIAL 1984, *Ann. Geophys.*, *6*, 39–50.

Whitney, H. E., J. Aarons, and C. Malik (1969), A proposed index for measuring ionospheric scintillations, *Planet. Space Sci.*, *17*(5), 1069–1073.

Wolf, R. A., R. W. Spiro, S. Sazykin, and F. R. Toffoletto (2007), How the Earth's inner magnetosphere works: An evolving picture, *J. Atmos. Sol. Terr. Phys.*, *69*(3), 288–302.